

Prandtl number effects in MRT Lattice Boltzmann models for shocked and unshocked compressible fluids

Feng Chen¹, Aiguo Xu^{2*}, Guangcai Zhang², Yingjun Li^{1†}

*1, State Key Laboratory for GeoMechanics and Deep Underground Engineering,
China University of Mining and Technology (Beijing), Beijing 100083*

*2, National Key Laboratory of Computational Physics,
Institute of Applied Physics and Computational Mathematics,
P. O. Box 8009-26, Beijing 100088, P.R.China*

(Dated: November 19, 2021)

Abstract

For compressible fluids under shock wave reaction, we have proposed two Multiple-Relaxation-Time (MRT) Lattice Boltzmann (LB) models [F. Chen, et al, EPL **90** (2010) 54003; Phys. Lett. A **375** (2011) 2129.]. In this paper, we construct a new MRT Lattice Boltzmann model which is not only for the shocked compressible fluids, but also for the unshocked compressible fluids. To make the model work for unshocked compressible fluids, a key step is to modify the collision operators of energy flux so that the viscous coefficient in momentum equation is consistent with that in energy equation even in the unshocked system. The unnecessary of the modification for systems under strong shock is analyzed. The model is validated by some well-known benchmark tests, including (i) thermal Couette flow, (ii) Riemann problem, (iii) Richtmyer-Meshkov instability. The first system is unshocked and the latter two are shocked. In all the three systems, the Prandtl number effects are checked. Satisfying agreements are obtained between new model results and analytical ones or other numerical results.

PACS numbers: 47.11.-j, 51.10.+y, 05.20.Dd

Keywords: lattice Boltzmann method; compressible flows; multiple-relaxation-time; Prandtl number; shock wave reaction

* Corresponding author. E-mail: Xu_Aiguo@iapcm.ac.cn

† Corresponding author. E-mail: lyj@aphy.iphy.ac.cn

I. INTRODUCTION

In recent years, the Lattice Boltzmann (LB) method has attracted much attention as a powerful tool in direct numerical simulation of fluid flows[1–3]. Unlike traditional computational fluid dynamics methods which solve macroscopic governing equations, the LB method employs the discrete Boltzmann equation which describes the fluid on the mesoscale level. This kinetic nature provides the LB method with essential physics.

However, there are also some limitations that restrict the applications of traditional LB method, such as the numerical stability problem, the fixed Prandtl number, and so on. The stability problem has been partly addressed by a number of techniques, such as the entropic method[4, 5], flux-limiter[6] and dissipation[7, 8] techniques. Besides these techniques, an effective method is the Multiple Relaxation Time (MRT) LB method[9–11], which employs multiple relaxation parameters in the collision step, instead of the commonly used Single Relaxation Time (SRT) collision. The flexibility gained from the MRT collision can be used to improve the stability property and overcome the fixed Prandtl number problem.

To the authors' knowledge, most of the existing MRT LB models work only for isothermal system[12–15], to cite but a few. To simulate system with temperature field, Luo, et al.[16] suggested a hybrid thermal MRT LB model, in which the mass and momentum equations are solved by the MRT model, whereas the diffusion-advection equation for the temperature is solved by Finite Difference (FD) technique or other means. Guo, et al.[17] proposed a coupling MRT LB model for thermal flows with viscous heat dissipation and compression work. Mezrhab, et al.[18] proposed a double MRT LB method, where MRT-D2Q9 model and the MRT-D2Q5 model are used to solve the flow and the temperature fields, respectively.

Besides the models mentioned above, we have proposed two MRT finite difference Lattice Boltzmann models for compressible fluids under shock in previous work[19, 20]. Numerical experiments showed that compressible flows with strong shocks can be well simulated by these models. In this paper, we further propose a new MRT Lattice Boltzmann model, which is not only for the shocked compressible fluids, but also for the unshocked compressible fluids. The rest of the paper is organized as follows: In Sec. II, we present the MRT LB model. The von Neumann stability analysis is given in Section III. Simulation results are presented and analyzed in Section IV. Section V makes the conclusion.

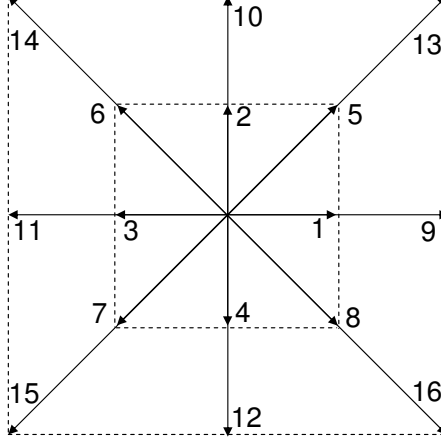


FIG. 1: Schematics of \mathbf{v}_i for the discrete velocity model.

II. DESCRIPTION OF THE MRT LB MODEL

In the MRT LB method, the evolution of the distribution function f_i is governed by the following equation

$$\frac{\partial f_i}{\partial t} + v_{i\alpha} \frac{\partial f_i}{\partial x_\alpha} = -\mathbf{M}_{il}^{-1} \hat{\mathbf{S}}_{lk} (\hat{f}_k - \hat{f}_k^{eq}), \quad (1)$$

where $v_{i\alpha}$ is the discrete particle velocity, $i = 1, \dots, N$, N is the number of discrete velocities, the subscript α indicates x or y . The variable t is time, x_α is the spatial coordinate. The matrix $\hat{\mathbf{S}} = \mathbf{M}\mathbf{S}\mathbf{M}^{-1} = \text{diag}(s_1, s_2, \dots, s_N)$ is the diagonal relaxation matrix, f_i and \hat{f}_i are the particle distribution function in the velocity space and the kinetic moment space respectively, $\hat{f}_i = m_{ij} f_j$, m_{ij} is an element of the transformation matrix \mathbf{M} . Obviously, the mapping between moment space and velocity space is defined by the linear transformation \mathbf{M} , i.e., $\hat{\mathbf{f}} = \mathbf{M}\mathbf{f}$, $\mathbf{f} = \mathbf{M}^{-1}\hat{\mathbf{f}}$, where the bold-face symbols denote N -dimensional column vectors, e.g., $\mathbf{f} = (f_1, f_2, \dots, f_N)^T$, $\hat{\mathbf{f}} = (\hat{f}_1, \hat{f}_2, \dots, \hat{f}_N)^T$, $\mathbf{M} = (m_1, m_2, \dots, m_N)^T$, $m_i = (m_{i1}, m_{i2}, \dots, m_{iN})$. \hat{f}_i^{eq} is the equilibrium value of the moment \hat{f}_i .

We construct a two-dimensional MRT LB model based on a 16-discrete-velocity model (see Fig. 1):

$$(v_{i1}, v_{i2}) = \begin{cases} \mathbf{cyc} : (\pm 1, 0), & \text{for } 1 \leq i \leq 4, \\ (\pm 1, \pm 1), & \text{for } 5 \leq i \leq 8, \\ \mathbf{cyc} : (\pm 2, 0), & \text{for } 9 \leq i \leq 12, \\ (\pm 2, \pm 2), & \text{for } 13 \leq i \leq 16, \end{cases}$$

where \mathbf{cyc} indicates the cyclic permutation.

The transformation matrix \mathbf{M} is constructed according to the irreducible representation bases of SO(2) group, and it can be expressed as follows:

$$\mathbf{M} = (m_1, m_2, \dots, m_{16})^T,$$

where

$$\begin{aligned} m_1 &= (1, 1, 1, 1, 1, 1, 1, 1, 1, 1, 1, 1, 1, 1, 1, 1), \\ m_2 &= (1, 0, -1, 0, 1, -1, -1, 1, 2, 0, -2, 0, 2, -2, -2, 2), \\ m_3 &= (0, 1, 0, -1, 1, 1, -1, -1, 0, 2, 0, -2, 2, 2, -2, -2), \\ m_4 &= \left(\frac{1}{2}, \frac{1}{2}, \frac{1}{2}, \frac{1}{2}, 1, 1, 1, 1, 2, 2, 2, 2, 4, 4, 4, 4\right), \\ m_5 &= (1, -1, 1, -1, 0, 0, 0, 0, 4, -4, 4, -4, 0, 0, 0, 0), \\ m_6 &= (0, 0, 0, 0, 1, -1, 1, -1, 0, 0, 0, 0, 4, -4, 4, -4), \\ m_7 &= \left(\frac{1}{2}, 0, -\frac{1}{2}, 0, 1, -1, -1, 1, 4, 0, -4, 0, 8, -8, -8, 8\right), \\ m_8 &= \left(0, \frac{1}{2}, 0, -\frac{1}{2}, 1, 1, -1, -1, 0, 4, 0, -4, 8, 8, -8, -8\right), \\ m_9 &= (1, 0, -1, 0, -2, 2, 2, -2, 8, 0, -8, 0, -16, 16, 16, -16), \\ m_{10} &= (0, -1, 0, 1, 2, 2, -2, -2, 0, -8, 0, 8, 16, 16, -16, -16), \\ m_{11} &= \left(\frac{1}{4}, \frac{1}{4}, \frac{1}{4}, \frac{1}{4}, 1, 1, 1, 1, 4, 4, 4, 4, 16, 16, 16, 16\right), \\ m_{12} &= (1, 1, 1, 1, -4, -4, -4, -4, 16, 16, 16, 16, -64, -64, -64, -64), \\ m_{13} &= (1, -1, 1, -1, 0, 0, 0, 0, 16, -16, 16, -16, 0, 0, 0, 0), \\ m_{14} &= (0, 0, 0, 0, 2, -2, 2, -2, 0, 0, 0, 0, 32, -32, 32, -32), \\ m_{15} &= (1, 0, -1, 0, -4, 4, 4, -4, 32, 0, -32, 0, -128, 128, 128, -128), \\ m_{16} &= (0, -1, 0, 1, 4, 4, -4, -4, 0, -32, 0, 32, 128, 128, -128, -128). \end{aligned}$$

For two-dimensional compressible models, we have four conserved moments, density ρ , momentums j_x , j_y , and energy e . They are denoted by \hat{f}_1 , \hat{f}_2 , \hat{f}_3 and \hat{f}_4 , respectively. Specifically, $\hat{f}_1 = \rho$, $\hat{f}_2 = j_x$, $\hat{f}_3 = j_y$, $\hat{f}_4 = e = \rho(T + u^2/2)$. Using the Chapman-Enskog expansion[13, 14, 21] on the two sides of LB equation, the Navier-Stokes (NS) equations for compressible fluids can be derived. The equilibria of the nonconserved moments can be chosen as

$$\hat{f}_5^{eq} = (j_x^2 - j_y^2)/\rho, \tag{2a}$$

$$\hat{f}_6^{eq} = j_x j_y / \rho, \quad (2b)$$

$$\hat{f}_7^{eq} = (e + \rho RT) j_x / \rho, \quad (2c)$$

$$\hat{f}_8^{eq} = (e + \rho RT) j_y / \rho, \quad (2d)$$

$$\hat{f}_9^{eq} = (j_x^2 - 3j_y^2) j_x / \rho^2, \quad (2e)$$

$$\hat{f}_{10}^{eq} = (3j_x^2 - j_y^2) j_y / \rho^2, \quad (2f)$$

$$\hat{f}_{11}^{eq} = 2e^2 / \rho - (j_x^2 + j_y^2)^2 / 4\rho^3, \quad (2g)$$

$$\hat{f}_{13}^{eq} = (6\rho e - 2j_x^2 - 2j_y^2)(j_x^2 - j_y^2) / \rho^3, \quad (2h)$$

$$\hat{f}_{14}^{eq} = (6\rho e - 2j_x^2 - 2j_y^2) j_x j_y / \rho^3. \quad (2i)$$

The recovered NS equations are as follows:

$$\frac{\partial \rho}{\partial t} + \frac{\partial j_x}{\partial x} + \frac{\partial j_y}{\partial y} = 0, \quad (3a)$$

$$\frac{\partial j_x}{\partial t} + \frac{\partial}{\partial x} (j_x^2 / \rho) + \frac{\partial}{\partial y} (j_x j_y / \rho) = -\frac{\partial P}{\partial x} + \frac{\partial}{\partial x} [\mu_s (\frac{\partial u_x}{\partial x} - \frac{\partial u_y}{\partial y})] + \frac{\partial}{\partial y} [\mu_v (\frac{\partial u_y}{\partial x} + \frac{\partial u_x}{\partial y})], \quad (3b)$$

$$\frac{\partial j_y}{\partial t} + \frac{\partial}{\partial x} (j_x j_y / \rho) + \frac{\partial}{\partial y} (j_y^2 / \rho) = -\frac{\partial P}{\partial y} + \frac{\partial}{\partial x} [\mu_v (\frac{\partial u_y}{\partial x} + \frac{\partial u_x}{\partial y})] - \frac{\partial}{\partial y} [\mu_s (\frac{\partial u_x}{\partial x} - \frac{\partial u_y}{\partial y})], \quad (3c)$$

$$\begin{aligned} & \frac{\partial e}{\partial t} + \frac{\partial}{\partial x} [(e + P) j_x / \rho] + \frac{\partial}{\partial y} [(e + P) j_y / \rho] \\ &= \frac{\partial}{\partial x} [\lambda_1 (R \frac{\partial T}{\partial x} + \frac{1}{2} (u_y \frac{\partial u_y}{\partial x} + u_x \frac{\partial u_x}{\partial x} - u_x \frac{\partial u_y}{\partial y} + u_y \frac{\partial u_x}{\partial y}))] \\ & \quad + \frac{\partial}{\partial y} [\lambda_2 (R \frac{\partial T}{\partial y} + \frac{1}{2} (u_x \frac{\partial u_x}{\partial y} - u_y \frac{\partial u_x}{\partial x} + u_x \frac{\partial u_y}{\partial x} + u_y \frac{\partial u_y}{\partial y}))], \end{aligned} \quad (3d)$$

where $\mu_s = \rho RT / s_5$, $\mu_v = \rho RT / s_6$, $\lambda_1 = 2\rho RT / s_7$, $\lambda_2 = 2\rho RT / s_8$.

When $\mu_s = \mu_v = \mu$, $\lambda_1 = \lambda_2 = \lambda$, the above NS equations reduce to

$$\frac{\partial \rho}{\partial t} + \frac{\partial j_\alpha}{\partial x_\alpha} = 0, \quad (4a)$$

$$\frac{\partial j_\alpha}{\partial t} + \frac{\partial (j_\alpha j_\beta / \rho)}{\partial x_\beta} = -\frac{\partial P}{\partial x_\alpha} + \frac{\partial}{\partial x_\beta} [\mu (\frac{\partial u_\alpha}{\partial x_\beta} + \frac{\partial u_\beta}{\partial x_\alpha} - \frac{\partial u_\chi}{\partial x_\chi} \delta_{\alpha\beta})], \quad (4b)$$

$$\frac{\partial e}{\partial t} + \frac{\partial}{\partial x_\alpha} [(e + P) j_\alpha / \rho] = \frac{\partial}{\partial x_\alpha} [\lambda (R \frac{\partial T}{\partial x_\alpha} + \frac{1}{2} u_\beta (\frac{\partial u_\alpha}{\partial x_\beta} + \frac{\partial u_\beta}{\partial x_\alpha} - \frac{\partial u_\chi}{\partial x_\chi} \delta_{\alpha\beta}))]. \quad (4c)$$

It should be pointed out that, the viscous coefficient in the energy equation (4c) is not consistent with that in the momentum equation (4b). Motivated by the idea of Guo et al. [17], the collision operators of the moments related to the energy flux are modified:

$$\hat{\mathbf{S}}_{77}(\hat{f}_7 - \hat{f}_7^{eq}) \Rightarrow \hat{\mathbf{S}}_{77}(\hat{f}_7 - \hat{f}_7^{eq}) + (s_7/s_5 - 1)\rho T u_x \left(\frac{\partial u_x}{\partial x} - \frac{\partial u_y}{\partial y} \right) + (s_7/s_6 - 1)\rho T u_y \left(\frac{\partial u_y}{\partial x} + \frac{\partial u_x}{\partial y} \right),$$

$$\hat{\mathbf{S}}_{88}(\hat{f}_8 - \hat{f}_8^{eq}) \Rightarrow \hat{\mathbf{S}}_{88}(\hat{f}_8 - \hat{f}_8^{eq}) + (s_8/s_6 - 1)\rho T u_x \left(\frac{\partial u_y}{\partial x} + \frac{\partial u_x}{\partial y} \right) + (s_8/s_5 - 1)\rho T u_y \left(\frac{\partial u_x}{\partial x} - \frac{\partial u_y}{\partial y} \right).$$

With this modification, we are able to get the following thermohydrodynamic equations:

$$\frac{\partial \rho}{\partial t} + \frac{\partial j_\alpha}{\partial x_\alpha} = 0, \quad (5a)$$

$$\frac{\partial j_\alpha}{\partial t} + \frac{\partial (j_\alpha j_\beta / \rho)}{\partial x_\beta} = -\frac{\partial P}{\partial x_\alpha} + \frac{\partial}{\partial x_\beta} \left[\mu \left(\frac{\partial u_\alpha}{\partial x_\beta} + \frac{\partial u_\beta}{\partial x_\alpha} - \frac{\partial u_\chi}{\partial x_\chi} \delta_{\alpha\beta} \right) \right], \quad (5b)$$

$$\frac{\partial e}{\partial t} + \frac{\partial}{\partial x_\alpha} [(e + P)j_\alpha / \rho] = \frac{\partial}{\partial x_\alpha} \left[\lambda R \frac{\partial T}{\partial x_\alpha} + \mu u_\beta \left(\frac{\partial u_\alpha}{\partial x_\beta} + \frac{\partial u_\beta}{\partial x_\alpha} - \frac{\partial u_\chi}{\partial x_\chi} \delta_{\alpha\beta} \right) \right]. \quad (5c)$$

This modification method is also suitable for our previous MRT models[19, 20]. The definitions of \hat{f}_{12}^{eq} , \hat{f}_{15}^{eq} , \hat{f}_{16}^{eq} have no effect on macroscopic equations, so the choices of the three moments are flexible. Now we give three different and typical formations: $\hat{f}_{12}^{eq} = \hat{f}_{15}^{eq} = \hat{f}_{16}^{eq} = 0$ (version 1); $\hat{f}_{12}^{eq} = 0$, $\hat{f}_{15}^{eq} = \rho u_x (-4 + 10T + 5u_x^2 - 5u_y^2)$, $\hat{f}_{16}^{eq} = \rho u_y (4 - 10T + 5u_x^2 - 5u_y^2)$ (version 2); $\hat{f}_{12}^{eq} = M_{12i} f_i^{\max}$, $\hat{f}_{15}^{eq} = M_{15i} f_i^{\max}$, $\hat{f}_{16}^{eq} = M_{16i} f_i^{\max}$, $f_i^{\max} = \rho / (2\pi T) \exp(-(v_{i\alpha} - u_\alpha)^2 / (2T))$ (version 3). In the second version, the MRT model reduces to the usual lattice BGK model in ref.[22] which uses a higher-order velocity expansion for Maxwellian-type equilibrium distribution, if all the relaxation parameters are set to be a single relaxation frequency s , namely $\mathbf{S} = s\mathbf{I}$.

III. STABILITY ANALYSIS

In this section, the von Neumann stability analysis[20] on the new MRT LB model is performed. In the stability analysis, we write the solution of FD LB equation in the form of Fourier series. If all the eigenvalues of the coefficient matrix are less than 1, the algorithm is stable. Coefficient matrix G_{ij} of the unmodified model can be expressed as follows,

$$G_{ij} = \delta_{ij} - \frac{v_{i\alpha} \Delta t}{2\Delta x_\alpha} (e^{i\mathbf{k}_\alpha \Delta x_\alpha} - e^{-i\mathbf{k}_\alpha \Delta x_\alpha}) \delta_{ij} + \frac{1}{2} \left(\frac{v_{i\alpha} \Delta t}{\Delta x_\alpha} \right)^2 (e^{i\mathbf{k}_\alpha \Delta x_\alpha} - 2 + e^{-i\mathbf{k}_\alpha \Delta x_\alpha}) \delta_{ij} - \Delta t \mathbf{M}_{il}^{-1} \hat{\mathbf{S}}_{lk} \left(\frac{\partial \hat{f}_k}{\partial f_j} - \frac{\partial \hat{f}_k^{eq}}{\partial f_j} \right), \quad (6)$$

where

$$\begin{aligned} \hat{f}_k &= \mathbf{M}_{kp} f_p, \\ \frac{\partial \hat{f}_k^{eq}}{\partial f_j} &= \frac{\partial \hat{f}_k^{eq}}{\partial \rho} \frac{\partial \rho}{\partial f_j} + \frac{\partial \hat{f}_k^{eq}}{\partial T} \frac{\partial T}{\partial f_j} + \frac{\partial \hat{f}_k^{eq}}{\partial u_\alpha} \frac{\partial u_\alpha}{\partial f_j}. \end{aligned} \quad (7)$$

Because of the modification of the collision operators, the coefficient matrix G_{ij} corresponding to energy flux should be replaced by

$$\begin{aligned} G_{ij} &= \delta_{ij} - \frac{v_{i\alpha} \Delta t}{2\Delta x_\alpha} (e^{ik_\alpha \Delta x_\alpha} - e^{-ik_\alpha \Delta x_\alpha}) \delta_{ij} + \frac{1}{2} \left(\frac{v_{i\alpha} \Delta t}{\Delta x_\alpha} \right)^2 (e^{ik_\alpha \Delta x_\alpha} - 2 \\ &+ e^{-ik_\alpha \Delta x_\alpha}) \delta_{ij} - \Delta t \mathbf{M}_{i7}^{-1} \{ \hat{\mathbf{S}}_{77} \left(\frac{\partial \hat{f}_7}{\partial f_j} - \frac{\partial \hat{f}_7^{eq}}{\partial f_j} \right) + \frac{\partial}{\partial f_j} [(s_7/s_5 - 1) \rho T u_x \left(\frac{\partial u_x}{\partial x} - \frac{\partial u_y}{\partial y} \right)] \\ &+ \frac{\partial}{\partial f_j} [(s_7/s_6 - 1) \rho T u_y \left(\frac{\partial u_y}{\partial x} + \frac{\partial u_x}{\partial y} \right)] \}, \end{aligned} \quad (8)$$

and

$$\begin{aligned} G_{ij} &= \delta_{ij} - \frac{v_{i\alpha} \Delta t}{2\Delta x_\alpha} (e^{ik_\alpha \Delta x_\alpha} - e^{-ik_\alpha \Delta x_\alpha}) \delta_{ij} + \frac{1}{2} \left(\frac{v_{i\alpha} \Delta t}{\Delta x_\alpha} \right)^2 (e^{ik_\alpha \Delta x_\alpha} - 2 \\ &+ e^{-ik_\alpha \Delta x_\alpha}) \delta_{ij} - \Delta t \mathbf{M}_{i8}^{-1} \{ \hat{\mathbf{S}}_{88} \left(\frac{\partial \hat{f}_8}{\partial f_j} - \frac{\partial \hat{f}_8^{eq}}{\partial f_j} \right) + \frac{\partial}{\partial f_j} [(s_8/s_6 - 1) \rho T u_x \left(\frac{\partial u_y}{\partial x} + \frac{\partial u_x}{\partial y} \right)] \\ &+ \frac{\partial}{\partial f_j} [(s_8/s_5 - 1) \rho T u_y \left(\frac{\partial u_x}{\partial x} - \frac{\partial u_y}{\partial y} \right)] \}. \end{aligned} \quad (9)$$

We conduct a quantitative analysis using the software, Mathematica. In Fig.2 we show some stability comparisons for the new MRT model, its SRT counterpart and our previous model in refs.[19, 20]. The abscissa is for kdx , and the vertical axis is for $|\omega|_{max}$ which is the largest eigenvalue of coefficient matrix G_{ij} . Grid sizes are $dx = dy = 10^{-3}$, and time step is $dt = 10^{-5}$, the relaxation frequency in SRT is $s = 10^5$. The other parameters in stability analysis are chosen as follows: (a), $(\rho, u_1, u_2, T) = (2.0, 2.0, 0.0, 2.0)$, the collision parameters in MRT are $s_i = 10^5, i = 1, \dots, 16$, the Mach number is 1 ($Ma = u/\sqrt{2T} = 2/2$); (b), $(\rho, u_1, u_2, T) = (2.0, 6.0, 0.0, 2.0)$, the collision parameters in the three versions are $s_9 = 10^3$, those in model[19] are $s_{10} = 5 \times 10^4, s_{11} = 2 \times 10^4, s_{13} = 1.5 \times 10^4$, and those in [20] are $s_9 = 8 \times 10^3, s_{13} = 7 \times 10^4, s_{14} = 5 \times 10^4$, the others are 10^5 , and the Mach number is 3.0; (c), $(\rho, u_1, u_2, T) = (2.0, 10.0, 0.0, 2.0)$, the collision parameters in the three versions are $s_9 = 1.2 \times 10^4, s_{13} = 10^2, s_{14} = 5 \times 10^4, s_{15} = 1.5 \times 10^3$, those in model[19] are $s_{13} = 1.5 \times 10^4$, and those in model[20] are $s_9 = 2 \times 10^3, s_{13} = 6.1 \times 10^4, s_{14} = s_{15} = 3 \times 10^4$, the others are 10^5 , and the Mach number is 5; (d), $(\rho, u_1, u_2, T) = (2.0, 12.0, 0.0, 2.0)$, the collision parameters in the three versions are $s_9 = 10^4, s_{13} = 10^2, s_{14} = 6 \times 10^4, s_{15} = 1.5 \times 10^3$,

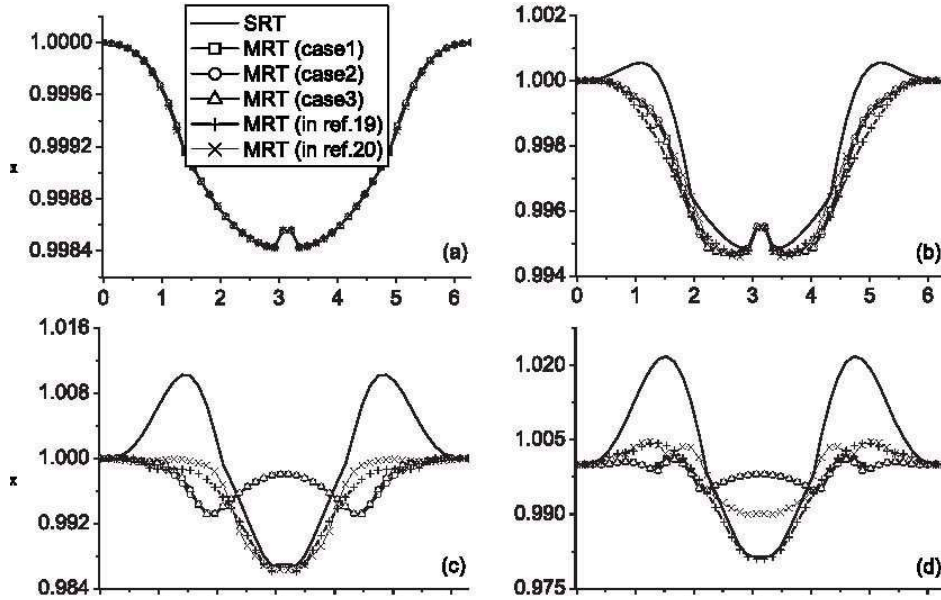


FIG. 2: Stability comparison for the new MRT model and its SRT counterpart.

and those in model[19] are $s_{11} = 2 \times 10^4$, $s_{13} = 1.5 \times 10^4$, and those in [20] are $s_9 = 10^3$, $s_{13} = 5 \times 10^3$, $s_{14} = s_{15} = 3 \times 10^4$, the others are 10^5 , and the Mach number is 6. In case (a), the MRT and SRT have the same stability; with the increase of Mach number (case (b) and (c)), the MRT models are stable, while the SRT version is not; if further increases the Mach number, MRT models also encounter instability problem (case (d)). It is clear that, by choosing appropriate collision parameters, the stability of MRT can be much better than the SRT. Three versions of the new MRT model do not show large differences in numerical stability.

IV. NUMERICAL SIMULATIONS

In this section, we study the following problems using the modified MRT LB model: Couette flow, One-dimensional Riemann problem, and Richtmyer-Meshkov instability. We work in a frame where the constant $R = 1$.

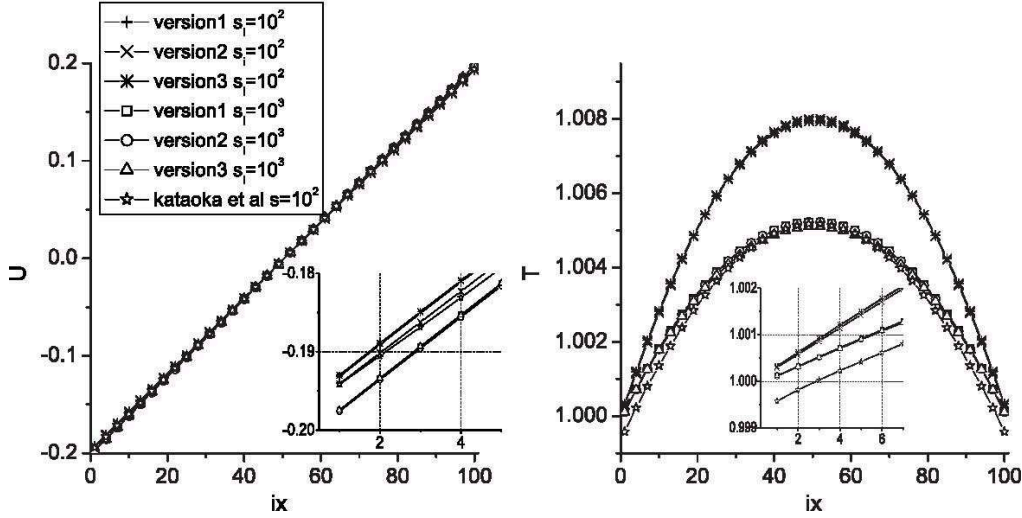


FIG. 3: Slip velocity and temperature jump simulated with the three versions and the model proposed by Kataoka, et al.

A. Unshocked compressible fluids

Here we conduct a series of numerical simulations of Couette flow. The aims of simulation of Couette flow are twofold. At first, we prove the Maxwellian property of the discrete equilibrium functions. Consider a viscous fluid flow between two parallel flat plates, moving in the opposite directions, $U_{wr} = -U_{wl} = 0.2$, where subscripts wr and wl indicate the walls in the right and left sides. The initial state of the fluid is $\rho = 1$, $T = 1$, $U = 0$. The temperatures of walls are $T_{wr} = T_{wl} = 1$. Near the walls, we adopt the diffuse reflection boundary conditions proposed by Sofonea, et al[23]. In the other two boundaries the periodic boundary condition is adopted. In the diffuse reflection boundary, the particles leaving the wall are assumed to follow the Maxwellian distribution. Following the discretization of the velocity space, in the FD LB model the Maxwellian distribution function is replaced by the equilibrium distribution function.

Fig. 3 shows the velocity and temperature profiles simulated with the three versions of this proposed model and the model proposed by Kataoka, et al[24]. The abscissa ix is the index of lattice node in the x - directions, and the vertical axes are velocity u and temperature T , respectively. The parameters are $dx = dy = 0.01$, $dt = 10^{-4}$, $NX \times NY = 100 \times 5$. The diffuse reflection boundary conditions work well with our model, the slip velocity and temperature jump near the walls are clearly seen, and increase with Knudsen number. While

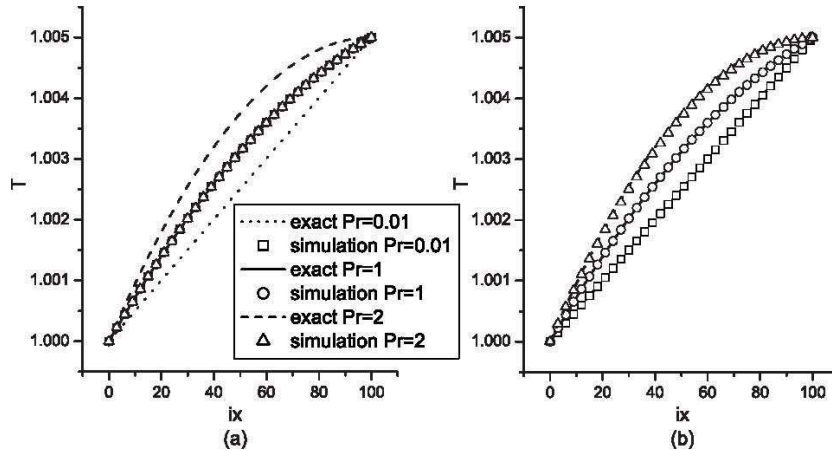


FIG. 4: Effects of heat conductivity on temperature profiles of Couette flow. (a) corresponds to the unmodified model(version 1), and (b) corresponds to the modified model. $Pr = 0.01$, $Pr = 1$ and $Pr = 2$ correspond to $s_7 = s_8 = 10$, $s_7 = s_8 = 10^3$, and $s_7 = s_8 = 2 \times 10^3$, respectively (other collision parameters are 10^3).

it fails to work for the model by Kataoka et al, because the temperature near the wall is lower than the wall temperature, which is contrary to physical idea. In Couette flow the fluid at the walls should have a higher temperature than the walls themselves, because of the heat generated by the viscous flow. We think this contradiction is caused from the equilibrium distribution function in their model which is not a Taylor expansion of the Maxwellian. So it departs from the basic assumption of diffuse reflection boundary. None of the three versions violates the basic assumption and destroys the Maxwellian property of the discrete equilibrium functions.

Secondly, we will compare the ability of the unmodified model and the modified model for the unshocked compressible fluids. In the simulation, the left wall is fixed and the right wall moves at speed $U = 0.1$. The simulation results are compared with the analytical solution:

$$T = T_1 + (T_2 - T_1)\frac{x}{H} + \frac{\mu}{2\lambda}U^2\frac{x}{H}\left(1 - \frac{x}{H}\right),$$

where T_1 and T_2 are the left and right wall's temperatures ($T_1 = 1$, $T_2 = 1.005$), H is the width of the channel. Other parameters remain unchanged. Periodic boundary conditions are applied to the bottom and top boundaries, and the left and right walls adopt the nonequilibrium extrapolation method. Fig. 4 and Fig. 5 show the temperature profiles of Couette flow simulated with the unmodified model (version 1) and its modified version.

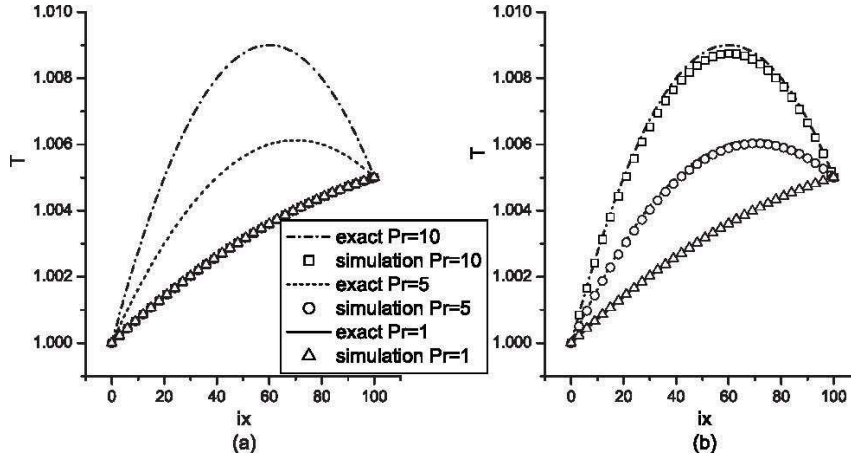


FIG. 5: Effects of viscosity on temperature profiles of Couette flow. (a) corresponds to the unmodified model (version 1), and (b) corresponds to the modified model. $Pr = 10$, $Pr = 5$ and $Pr = 1$ correspond to $s_5 = s_6 = 10^2$, $s_5 = s_6 = 2 \times 10^2$, and $s_5 = s_6 = 10^3$, respectively (other collision parameters are 10^3).

In Fig. 4, we fix viscosity coefficient $s_5 = s_6 = 10^3$, and change the thermal conductivity $s_7 = s_8$ from 10 to 2×10^3 . On the contrary, we fix thermal conductivity $s_7 = s_8 = 10^3$, and change the viscosity $s_5 = s_6$ from 10^2 to 10^3 in Fig. 5. (a) corresponds to the unmodified model (version 1), and (b) corresponds to the modified model. It is clearly shown that the simulation results of modified model are in agreement with the analytical solutions, and the Prandtl number effects on unshocked compressible fluids are successfully captured by the modified model, but not by the unmodified model.

B. Shocked compressible fluids

(a) Riemann problem

Here we construct a high Mach number shock tube problem with the initial condition,

$$\begin{cases} (\rho, u_1, u_2, T)|_L = (5.0, 45.0, 0.0, 10.0), & x \leq 0. \\ (\rho, u_1, u_2, T)|_R = (6.0, -20.0, 0.0, 5.0), & x > 0. \end{cases} \quad (10)$$

The Mach number of the left side is 10.1 ($Ma = u/\sqrt{2T} = 45/\sqrt{20}$), and the right is 6.3 ($Ma = u/\sqrt{2T} = 20/\sqrt{10}$). Figure 6 shows the comparison of LB results and exact solutions at $t = 0.018$, where the parameters are $dx = dy = 0.003$, $dt = 10^{-5}$, $s_5 = s_6 = 1.5 \times 10^4$,

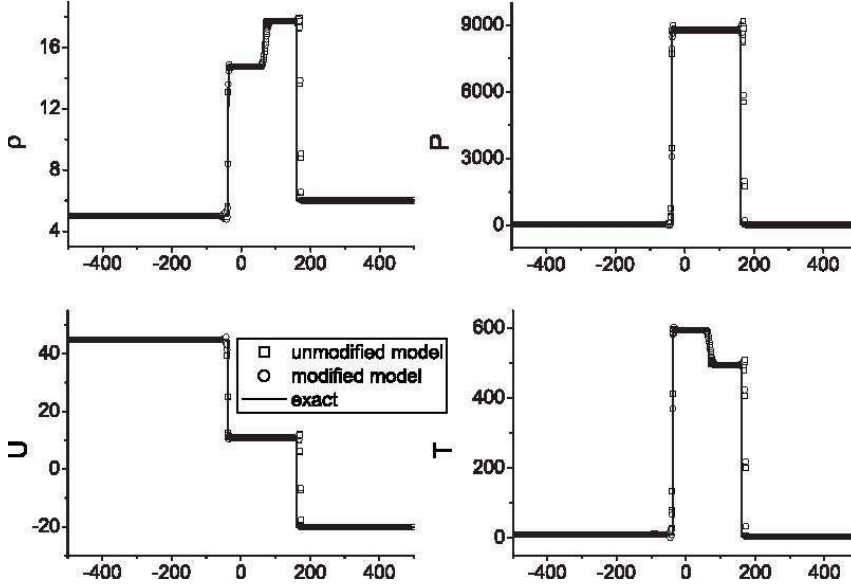


FIG. 6: LB results and exact solutions for shock tube problem at time $t = 0.018$. ρ : density, P : pressure, U : the x - component of velocity, T : temperature.

other values of s are 10^5 . Squares correspond to simulation results with the unmodified model (version 1), the circle symbols correspond to the modified MRT simulation results, and solid lines represent the exact solutions, respectively. It can be seen that the simulations of the two MRT models do not show large differences. For shocked compressible flows, there exist a fast procedure and a slow one. The shock dynamic procedure is fast, while that of heat conduction is slow. In such a case, from the view of macroscopic description, the terms related to viscosity and heat conductivity may be neglected. So, terms related to viscosity and heat conductivity in Eqs.(3) and (5) are all small terms and make negligible effects. That is the reason why the unmodified model works also well in such cases.

(b) Richtmyer-Meshkov instability

The Richtmyer-Meshkov (RM) instability[25, 26] is a fundamental fluid instability that develops when an incident shock wave collides with an interface between two fluids with different densities. This instability is involved in numerous physical processes, such as inertial confined fusion, supersonic and hypersonic combustion, supernova explosion, and so on. RM instability has attracted considerable attention for several decades because of its important theoretical and practical significance. To the best of our knowledge, the research

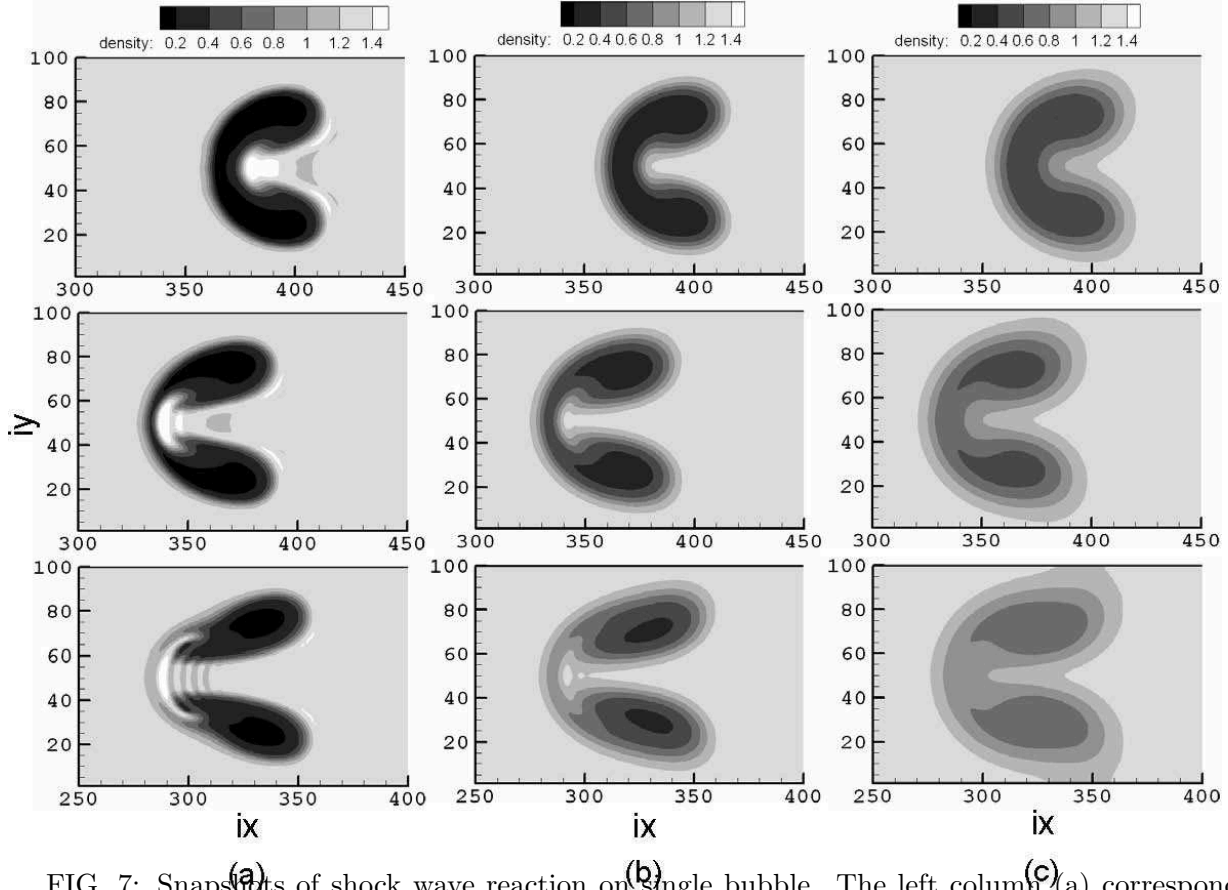


FIG. 7: Snapshots of shock wave reaction on single bubble. The left column (a) corresponds to $s_5 = s_6 = 10^4, s_7 = s_8 = 10^5$, the middle column (b) corresponds to $s_5 = s_6 = 10^4, s_7 = s_8 = 10^4$, and the right column (c) corresponds to $s_5 = s_6 = 10^4, s_7 = s_8 = 10^3$. From black to white the grey level corresponds to the increase of density.

of RM instability by LB method is still very limited. In this paper, we study the thermal conductivity and viscosity effects on RM instability with the MRT LB method.

The investigation of the interaction of a planar shock with an isolated gas bubble is of special significance in the study of RM instability, because the interface of gas bubble has typical three dimensional characteristic and large initial distortion. It helps to understand the mechanism of RM instability process. The problem we simulated is as follows: A planar shock wave with the Mach number 1.22 ($D = 1.725$), traveling from the right side, impinges

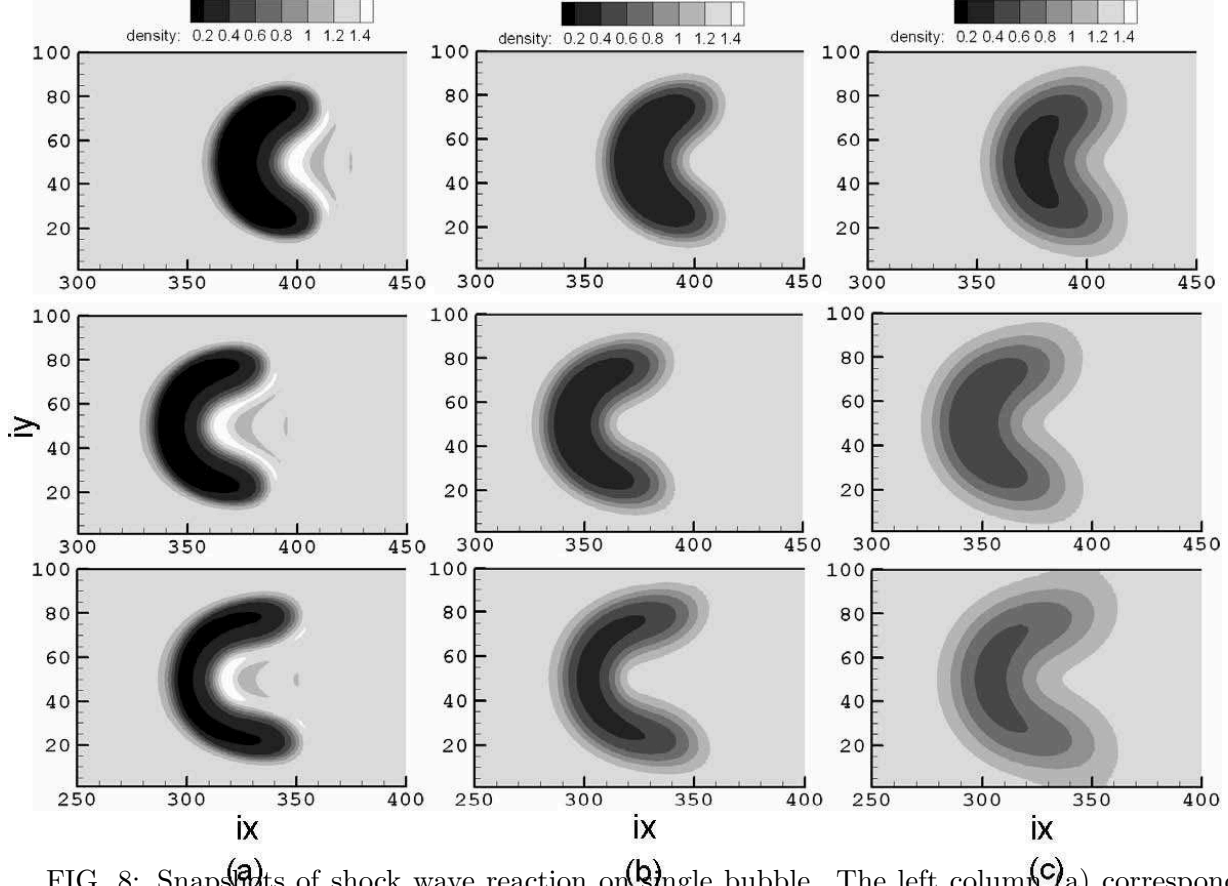


FIG. 8: Snapshots of shock wave reaction on single bubble. The left column (a) corresponds to $s_5 = s_6 = 10^3, s_7 = s_8 = 10^5$, the middle column (b) corresponds to $s_5 = s_6 = 10^3, s_7 = s_8 = 10^4$, and the right column (c) corresponds to $s_5 = s_6 = 10^3, s_7 = s_8 = 10^3$. From black to white the grey level corresponds to the increase of density.

on a cylindrical bubble. The initial macroscopic quantities are as follows:

$$(\rho, u_1, u_2, p) |_{x,y,0} = \begin{cases} (1, 0, 0, 1), & \text{pre - shock,} \\ (1.28, -0.3774, 0, 1.6512), & \text{post - shock,} \\ (0.1358, 0, 0, 1), & \text{bubble,} \end{cases} \quad (11)$$

The domain of computation is a rectangle $Nx \times Ny = 600 \times 100$, Nx and Ny are the numbers of lattice node in the x - and y - directions. Initially, the bubble is at the position $(450, 50)$, the post-shock domain is $[501, 600] \times [0, 100]$. In the simulations, the right side adopts the initial values of post-shock flow, the extrapolation technique is applied at the left boundary, and reflection conditions are imposed on the other two surfaces.

In Figures 7 and 8, we show some simulation results with different configurations. The abscissa is for ix , and the vertical axis is for iy , where ix and iy are the indexes of lattice node in the x - and y - directions. From top to bottom, the three rows show the density contours at times $t = 0.5, 0.7, 1$, respectively. The common parameters are $dx = dy = 0.003$, $dt = 10^{-5}$. The collision parameters in Fig. 7(a) are $s_5 = s_6 = 10^4$, $s_7 = s_8 = 10^5$, those in Fig. 7(b) are $s_5 = s_6 = 10^4$, $s_7 = s_8 = 10^4$, and those in Fig. 7(c) are $s_5 = s_6 = 10^4$, $s_7 = s_8 = 10^3$, 10^5 for the others. The collision parameters in Fig. 8(a) are $s_5 = s_6 = 10^3$, $s_7 = s_8 = 10^5$, those in Fig. 8(b) are $s_5 = s_6 = 10^3$, $s_7 = s_8 = 10^4$, and those in Fig. 8(c) are $s_5 = s_6 = 10^3$, $s_7 = s_8 = 10^3$, 10^5 for the others. Fig. 7 and Fig. 8 show that when the viscosity is constant, the small thermal conductivity is beneficial to the development of RM instability. Comparing Fig. 7 with Fig. 8, we find when the thermal conductivity is constant, the small viscosity is beneficial to the development of RM instability. The thermal conductivity and viscosity have inhibition effects on the development of RM instability. Both the unmodified model and the modified model get the same results.

V. CONCLUSIONS

We propose a MRT Lattice Boltzmann model which works not only for the shocked compressible fluids but also for the unshocked compressible fluids. In the new model, a key step is the modification of the collision operators of energy flux so that viscous coefficient in momentum equation and that in energy equation are consistent no matter if the system is shocked or not. The unnecessary of the modification for systems under strong shock is analyzed. The new model is validated by some well-known benchmark tests, including (i) thermal Couette flow, (ii) Riemann problem, (iii) Richtmyer-Meshkov instability. The first system is unshocked and the latter two are shocked. In all the three systems, the Prandtl numbers effects are checked. Satisfying agreements are obtained between the new model results and analytical ones or other numerical results. Our previous models[19, 20] can be revised in the same way to simulate unshocked compressible flows.

Acknowledgements

This work is supported by the Science Foundations of LCP and CAEP [under Grant Nos. 2009A0102005, 2009B0101012], National Basic Research Program of China [under Grant No. 2007CB815105], National Natural Science Foundation of China [under Grant Nos. 11071024, 11075021 and 11074300], the Fundamental Research Funds for the Central Universities [under Grant No. 2010YS03].

-
- [1] S. Succi, *The Lattice Boltzmann Equation for Fluid Dynamics and Beyond*, Oxford University Press, New York (2001).
 - [2] R. Benzi, S. Succi, and M. Vergassola, *Phys. Rep.* **222** (1992) 145.
 - [3] Aiguo Xu, G. Gonnella, and A. Lamura, *Phys. Rev. E* **67** (2003) 056105; *Phys. Rev. E* **74** (2006) 011505; *Physica A* **331** (2004) 10; *Physica A* **344** (2004) 750; *Physica A* **362** (2006) 42.
 - [4] F. Tosi, S. Ubertini, S. Succi, H. Chen, and I. V. Karlin, *Math. Comput. Simul.* **72** (2006) 227.
 - [5] S. Ansumali, I.V. Karlin, *J. Stat. Phys.* **107** (2002) 291.
 - [6] V. Sofonea, A. Lamura, G. Gonnella, and A. Cristea, *Phys. Rev. E* **70** (2004) 046702.
 - [7] X. F. Pan, Aiguo Xu, and Guangcai Zhang, S. Jiang, *Int. J. Mod. Phys. C* **18** (2007) 1747; Y. Gan, Aiguo Xu, Guangcai Zhang, X. Yu, and Y. Li, *Physica A* **387** (2008) 1721.
 - [8] R. A. Brownlee, A. N. Gorban, J. Levesley, *Phys. Rev. E* **75** (2007) 036711.
 - [9] F. J. Higuera, S. Succi, and R. Benzi, *Europhys. Lett.* **9** (1989) 345. F. J. Higuera, J. Jimenez, *Europhys. Lett.* **9** (1989) 662.
 - [10] D. d’Humières, *Generalized lattice-Boltzmann equations*, in *Rarefied Gas Dynamics: Theory and Simulations*, edited by B. D. Shizgal and D. P Weaver, Progress in Astronautics and Aeronautics, Vol. 159(AIAA Press, Washington, DC, 1992), pp450-458.
 - [11] R. Adhikari, S. Succi, *Phys. Rev. E* **78** (2008) 066701.
 - [12] P. Lallemand, L. S. Luo, *Phys. Rev. E* **61** (2000) 6546.
 - [13] R. Du, B. Shi, and X. Chen, *Phys. Lett. A* **359** (2006) 564.
 - [14] M. E. McCracken, J. Abraham, *Phys. Rev. E* **71** (2005) 036701.

- [15] L. Zheng, Z.L. Guo, B.C. Shi, and C.G. Zheng, Phys. Rev. E **81** (2010) 016706.
- [16] P. Lallemand, L. S. Luo, Phys. Rev. E **68** (2003) 036706.
- [17] L. Zheng, B.C. Shi, Z.L. Guo, Phys. Rev. E **78** (2008) 026705.
- [18] A. Mezrhab, M. A. Moussaouia, M. Jami, H. Naji, and M. Bouzidi, Physics Letters A **374** (2010) 3499.
- [19] F. Chen, Aiguo Xu, G. C. Zhang, Y. J. Li, and S. Succi, Europhys. Lett. **90** (2010) 54003.
- [20] F. Chen, Aiguo Xu, G. C. Zhang, Y. J. Li, Physics Letters A **375** (2011) 2129.
- [21] S. Chapman and T.G. Cowling, *The mathematical theory of non-uniform gases*, Cambridge University Press, London (1970).
- [22] Y. Chen, H. Ohashi, and M. Akiyama, Phys. Rev. E **50** (1994) 2776.
- [23] V. Sofonea, and R. F. Sekerka, Phys. Rev. E **71** (2005) 066709.
- [24] T. Kataoka, M. Tsutahara, Phys. Rev. E **69** (2004) 035701(R).
- [25] R. D. Richtmyer, Commun. Pure Appl. Maths. **8** (1960) 297.
- [26] E. E. Meshkov, Sov. Fluid Dyn. **4** (1969) 101.